Title

3D-Printed Coronary Implants Are Effective for Percutaneous Creation of Swine Models with Focal Coronary Stenosis.

Journal

Journal of Cardiovascular Translational Research, 13(6)

Authors

Colbert, Caroline
Shao, Jiaxin
Duarte-Vogel, Sandra
et al.

Publication Date

2020-12-01

DOI

10.1007/s12265-020-10018-3

Peer reviewed

Published in final edited form as:
J Cardiovasc Transl Res. 2020 December ; 13(6): 1033–1043. doi:10.1007/s12265-020-10018-3.

3D-Printed Coronary Implants are Effective for Percutaneous Creation of Swine Models with Focal Coronary Stenosis

Caroline M. Colbert, BS[1], **Jiaxin Shao, PhD**[2], **John J. Hollowed, MD**[3], **Jesse W. Currier, MD**[3], **Olujimi A. Ajijola, MD, PhD**[4], **Gregory A. Fishbein, MD**[5], **Sandra M. Duarte-Vogel, DVM**[6], **Rohan Dharmakumar, PhD**[7], **Peng Hu, PhD**[1,2], **Kim-Lien Nguyen, MD**[1,2,3]

[1]Physics and Biology in Medicine Graduate Program, David Geffen School of Medicine at UCLA. Los Angeles, CA.

[2]Diagnostic Cardiovascular Imaging Laboratory, Department of Radiological Sciences, David Geffen School of Medicine at UCLA.

[3]Division of Cardiology, David Geffen School of Medicine at UCLA and VA Greater Los Angeles Healthcare System. Los Angeles, CA.

[4]UCLA Cardiac Arrhythmia Center and Division of Cardiology, David Geffen School of Medicine at UCLA

[5]Department of Pathology, David Geffen School of Medicine at UCLA

[6]Division of Laboratory Animal Medicine, David Geffen School of Medicine at UCLA

[7]Department of Medicine, David Geffen School of Medicine at UCLA and Biomedical Imaging Research Institute, Cedars-Sinai Medical Center, Los Angeles, CA.

Abstract

Reliable, closed-chest methods for creating large animal models of acute myocardial hypoperfusion are limited. We demonstrated the feasibility and efficacy of using magnetic resonance (MR)-compatible 3D printed coronary implants for establishing swine models of myocardial hypoperfusion. We designed, manufactured, and percutaneously deployed implants in 13 swine to selectively create focal coronary stenosis. To test the efficacy of the implants to cause hypoperfusion or ischemia in the perfused territory, we evaluated regional wall motion, myocardial perfusion, and infarction using MR imaging. The overall swine survival rate was 85%

Address correspondence to: Kim-Lien Nguyen, MD, David Geffen School of Medicine at UCLA, VA Greater Los Angeles Healthcare System, 11301 Wilshire Blvd, MC 111E, Los Angeles, CA 90073, Phone: 310.592.0386, Fax: 310.268.3258, klnguyen@ucla.edu.

Author Contributions: Conception and design (KLN, PH, CMC), analysis and interpretation (CMC, KLN), data collection (CMC, KLN, JS, JHH, JWC, OAA, SMD, GAF), drafting the article (CMC, KLN), critical revision of the article (all authors), final approval of the article (all authors), overall responsibility (KLN).

Disclosures: The authors have no relevant conflicts of interest to disclose.

Human Studies: No human studies were carried out by the authors for this article.

Animal Studies: All institutional and national guidelines for the care and use of laboratory animals were followed and approved by our Institutional Animal Care and Use Committee (protocol #015–03D). With permission, S&S Farms supplied swine models purposely bred for biomedical research. S&S Farms Domestic pigs are a Yorkshire/Landrace hybrid originally derived from a specific pathogen free herd.

Competing interests: The authors declare no competing interests.

(11 of 13). The implant retrieval rate was 92% (12 of 13). Fluoroscopic angiography confirmed focal stenosis. Cine and perfusion MRI showed regional wall motion abnormalities and inducible ischemia, respectively. Late gadolinium enhancement and histopathology showed no myocardial infarction. Our minimally invasive technique has promising applications for validation of new diagnostic methods in cardiac MR.

Keywords

MRI; stress testing; acute swine model; ischemic heart disease; 3D printing; minimally invasive; animal models of human disease; ischemia; Magnetic Resonance Imaging (MRI); coronary circulation; translational studies

Introduction

Animal models of acute and chronic coronary stenosis for translational magnetic resonance imaging (MRI) have been developed using both open- and closed-chest techniques. The most popular open-chest method relies on ameroid constrictors [2–4], which are small, rounded clamps that can be fixed around an exposed coronary artery, restricting its diameter [3]. Deploying ameroid constrictors can be logistically difficult, requiring aseptic surgery to expose the coronary artery, placement of the constrictor on a beating heart, and closure of the pericardium and chest [2]. A minimum recovery period of 10 days is recommended and a recovery period of seven weeks is typically observed [2, 5–7]. While ameroid constrictors have the benefit of not introducing any foreign object into the vasculature, open-chest surgery may confound the results of acute investigations. Alternatively, a closed-chest method has been used to create acute focal coronary stenosis in swine models by implanting tapered nylon coronary flow reducers [8, 9]. These flow reducers are challenging to manufacture, and Kraitchman et al. report a relatively low success rate [8]. Other published closed-chest methods include injury models [10], modified covered stents [11, 12], and partially-inflated angioplasty balloons [13, 14]. Each of these methods has its own advantages and disadvantages.

In recent years, 3D printing technology has found increased adoption in cardiovascular research and clinical practice as a tool for education and intervention planning [15–17]. 3D printing shows promise for the development of vascular grafts, heart valves and cardiac muscle tissues in surgical interventions [18, 19], but consensus, workflow, reimbursements, and safety are barriers to widespread and routine clinical use. Because 3D printing can use a variety of MR compatible resins and bio-inks, researchers recently pioneered a percutaneous approach for delivery of rapid prototypes such as 3D printed implants into vascular lumen [20].

Despite increasing research and clinical applications, 3D printing has not been used to facilitate creation of large animal models with coronary stenosis. In the setting of coronary stenosis, myocardial hypoperfusion results. With further blood flow obstruction, myocardial ischemia in the segment subtended by the obstructed coronary vessel will ensue [21]. To diagnose obstructive coronary disease, exercise or pharmacologic stress perfusion MRI can be performed to document inducible ischemia [22]. The availability of an MRI-compatible,

minimally-invasive, relatively inexpensive, closed-chest acute swine model would facilitate more rapid, cost-effective, translational research in IHD. In this work, we sought to develop a closed-chest swine model of IHD using high-resolution 3D printed epicardial coronary implants to create focal, artificial coronary stenoses. Based on quantitative coronary angiography, in-vivo cardiac MRI and gross pathology, we aim to demonstrate the feasibility and efficacy of our new minimally invasive, rapid prototyping technique.

Materials and Methods

Experimental Animal Care and Use

Our Institutional Animal Care and Use Committee, the UCLA Chancellor's Animal Research Committee (ARC), approved the animal study protocol (IACUC #015–03D). We conducted the experiments according to guidelines set forth by the Guide for the Care and use of Laboratory Animals, the Animal Welfare Act, the National Institutes of Health, and the American Heart Association on Research Animal Use. Thirteen 25 – 40 kg adult male Yorkshire swine (S&S Farms, Ramona, CA) were housed for two weeks prior to experiments with no more than one pen mate in a dedicated vivarium staffed by certified veterinary technicians.

Design and manufacturing of heparin-coated epicardial coronary implant

Our intracoronary stenosis implants were designed to fit securely in the mid to distal left anterior descending artery (LAD), causing an acute coronary narrowing after percutaneous deployment. The 3D printed implant design reflected the shape, contour, and caliber of coronary vessels and had rounded edges to minimize potential for vessel injury (Fig. 1 a–d). A library of implant sizes with a range of inner diameter, outer diameter, and length was available for use in the catheterization lab. An appropriately-sized implant was selected in the cath lab based on swine coronary size, coronary guide catheter diameter, and degree of desired stenosis. We designed intracoronary implants using Autodesk Tinkercad (Autodesk Inc., San Rafael, California). Our in-house fabrication lab (LuxLab, UCLA) printed the implants from Formlabs grey resin (RS-F2-GPGR-04, Formlabs Inc., Somerville, MA) using a Formlabs Form 2 3D printer with a minimum XY feature size of 150 μm. Formlabs grey resin was chosen over more flexible commercial 3D printing resins to minimize compressibility, preventing collapse of the implant following deployment. After printing, we removed support materials that were created as part of the 3D printed proofs. To prevent thrombus formation, implants were dip-coated in a 25% heparin solution (Surface Solutions Laboratories, Inc., Carlisle, MA) with an aziridine crosslinker and allowed to air-dry for 24 hours. For quality control of the implants and to ensure minimal change in the dimensions of the implants, we visually inspected each implant for surface imperfections using a magnifying glass and measured the length, inner diameter and outer diameter of the implants following the application of the heparin coating using digital calipers (Clockwise Tools, Valencia, CA). A limited set of pin gages (Deltronic, Santa Ana, CA) were used to confirm the nominal accuracy of the digital caliper measurements.

Deployment of implant into swine models and fluoroscopic evaluation of implant location and extent of coronary narrowing

Prior to all procedures, Yorkshire pigs (25–40 kg male; S&S Farms, Ramona, CA) were sedated with intramuscular ketamine (10mg/kg) and midazolam (1mg/kg) and intubated. Inhaled 1–2% isoflurane and intravenous rocuronium (2.5mg/kg/hr) were used to achieve anesthesia and diaphragmatic muscle immobilization, a requirement for optimal cardiac image acquisition. Swine were ventilated with an oxygen-isoflurane (1–2%) mixture and maintained at a surgical plane of anesthesia throughout the procedures. Continuous vital signs, pCO2 levels, and single lead EKG were monitored.

After femoral arterial access and anticoagulation with intravenous heparin (5000–10000 units to achieve a target activated clotting time >350 s), we engaged the left main coronary artery using a guide catheter under fluoroscopic guidance. We assembled the implant deployment apparatus by 1) nesting a deflated, over-the-wire, coronary balloon angioplasty catheter (NC Trek, Abbott Laboratories, Abbott Park, Illinois, USA) within a mother-and-child catheter (GuideLiner, Teleflex, Minneapolis, MN, USA), 2) mounting the implant onto the angioplasty balloon, and 3) inflating the balloon to 2–3 atmospheres to stabilize the implant's position between radiographic markers on the angioplasty balloon [20]. Under fluoroscopic guidance, we advanced the assembled implant-balloon-loaded-mother-and-child catheter to the vessel of interest, positioned the implant in the targeted segment, and acquired angiograms to assess the stability of the implant position. We then deflated and retracted the balloon through the mother-and-child catheter, leaving the implant in place. We performed angiograms in orthogonal views to document the new artificial stenosis within the vessel and to estimate the severity of stenosis. We deployed implants in either the mid to distal LAD (left anterior descending coronary artery) or mid LCX (left circumflex coronary artery).

MRI for evaluation of implant-induced regional wall motion abnormalities, myocardial perfusion, and infarction.

Regional wall motion abnormalities, such as myocardial hypokinesis and akinesis, indicate hypoperfusion and ischemia in the territory targeted by the implanted coronary stenosis. To assess for the aforementioned surrogates of myocardial perfusion, we initiated MR imaging within one hour of femoral arterial access. We used a whole body, 3.0 Tesla clinical magnet (Prisma, Siemens, Germany) equipped with phased-array coils. The image acquisition protocol is shown in Fig. 1e. After initial localizers, we acquired short- and long-axis cine images using a gradient-echo sequence to evaluate regional wall motion of the left ventricle (n=13). [Field of view (FOV) = 292 × 360 mm, matrix size = 102 × 126, repetition time (TR) = 5.22 ms, echo time (TE)= 2.48 ms, slice thickness = 6 mm, pixel bandwidth = 450 Hz, flip angle = 12°].

To visualize myocardial perfusion defects caused by the implanted stenosis, we performed gadolinium-enhanced first pass perfusion imaging (n=6; gadobutrol, Gadavist, Bayer, Whippany, NJ, USA; 0.1 mmol/kg, 5 ml/sec at rest and at peak stress) under conditions of rest and at peak pharmacologic stress (n=6; adenosine, 300 μg/kg/min, 4 min infusion) [23]. Inducible myocardial ischemia is indicated by the presence of a visible perfusion

defect at stress and the absence of a perfusion defect at rest or by a rest perfusion defect that increases in extent at peak stress. We used a spoiled-gradient-echo perfusion sequence with representative parameters: FOV = 320 × 320 mm, slice thickness = 10 mm, matrix size = 130 × 130, TR = 2.5 ms, TE = 1.1 ms, pixel bandwidth = 650 Hz, flip angle = 12°. To exclude the presence of acute myocardial infarction in the segment subtended by the artificial coronary stenosis, we performed late gadolinium enhancement (LGE) imaging (n=6) using an ECG-gated, segmented, spoiled gradient-echo phase-sensitive-inversion-recovery sequence [FOV = 225 × 340 mm, slice thickness = 8 mm, matrix size = 131 × 175 mm, TR = 5.2 ms, TE = 1.96 ms, inversion time (TI) =optimized to null the myocardium, pixel bandwidth = 465 Hz, flip angle = 20°] at 10 minutes after the second bolus of gadolinium infusion.

Stenosis implant retrieval and post-mortem tissue histopathology examination

After MR image acquisition, we immediately euthanized the swine using sodium pentobarbital (100 mg/kg). We performed a lateral thoracotomy, excised the heart, and exposed the coronary arterial vasculature. After careful dissection of the coronary vessel, we located the epicardial coronary implant by visual inspection. We removed and inspected the implants for intraluminal thrombus formation. We evaluated the exposed coronary vessel for abrasions by gross inspection. We rinsed explanted hearts from three subjects in saline, sliced the ventricles parallel to the atrioventricular sulcus from apex to base (~1cm thickness), digitally photographed the fresh tissue, and then incubated the slices in 1% solution triphenyltetrazolium chloride (TTC) buffered in 0.2 M Tris buffer (pH 7.8) at 37°C for 5–7 minutes as previously described [24]. TTC staining causes regions of viable myocardium to appear deep or dark red, and infarcted /necrotic regions bright white. Previous work has shown that the spatial extent of enhancement on LGE images correlates closely ($r > 0.95$) with the spatial extent of infarction on TTC staining [25].

Image analysis and statistics

In order to compare the dimensions of the implanted stenosis with the degree of coronary narrowing visible on angiograms, vessel diameter and minimum lumen diameter were quantified in orthogonal fluoroscopic images using the Osirix DICOM viewer (Pixmeo, Bernex, Switzerland), with the guide catheter as a size reference (n=12). Percent diameter stenosis was evaluated relative to a reference vessel diameter immediately proximal to the implant, as previously described [11]. A reader (>8 years' experience in cardiovascular MRI and perfusion imaging and who had no identifying information about the location of coronary implant placement) visually inspected the first-pass perfusion images for perfusion defects (ischemia) and evaluated the LGE images for the presence or absence of myocardial infarction using a commercially available software (Argus, Siemens, Erhlangen, Germany). We visually assessed the cine images for regional wall motion abnormalities and performed quantitative feature-tracking strain analysis (n=8 swine subjects, TomTec, 2D CPA MR). Data are summarized as mean ± standard deviation (SD). Data ranges are included where appropriate. For group comparisons of segmental circumferential strain, we used a two-tailed paired Student's t-test (MedCalc v19.1, Belgium). A p value of <0.05 was considered significant.

Results

Intracoronary Stenosis Implant Sizing

We created a library of coronary implants with a range of dimensions to facilitate ease of intra-operative sizing. Based on the range of swine size and the diameter of an 8F coronary guide catheter used during the experiments, the outer diameter of the implants was limited to 2.1 mm. The minimum wall thickness of the implant was 0.3 mm and their length ranged from 2.6 to 4.0 mm. Digital caliper measurements found a mean deviation from nominal implant dimensions of −0.03±0.07 mm in length, 0.00±0.06 mm in outer diameter and −0.39±0.06 mm in inner diameter following application of the heparin coating. Application of the heparin coating caused a decrease in implant inner diameter of 0.09±0.11 mm on average.

Swine survival outcomes and quantitative analysis of coronary stenosis

We deployed 13 implants in 13 swine subjects. Following implant deployment, subjects showed a median baseline heart rate of 80 bpm (beats per minute, IQR 76 – 84), systolic blood pressure (SBP) of 98 mmHg (IQR 88 – 104) and diastolic blood pressure (DBP) of 56 mmHg (IQR 51 – 62). A summary of swine subject outcomes is presented in Table 1. The overall animal survival rate was 85% (11 of 13). One subject developed ventricular fibrillation; one became profoundly hypotensive and died. The swine models were hemodynamically stable post-implant, completed all imaging study procedures, and survived for at least 6 hours (from implant deployment to euthanasia). We were able confirm successful deployment by retrieving the implant in 12 of 13 subjects (92%). Subject outcomes improved over the course of the study. Of the first six cases, three were fully successful (deployment, retrieval, and subject survival until completion of imaging). All of the latter seven cases were fully successful. During the first six cases, each implant deployment took approximately one hour to complete. During the latter seven, improvements in our deployment technique allowed us to complete implant deployment in less than 30 minutes.

Quantitative analysis of post-deployment fluoroscopic angiograms showed focal coronary stenosis severity ranging from 40.6% to 62.7% (mean stenosis 56.8±7.0%, n=12 swine subjects). The mean minimum luminal diameter was 0.75±0.13 mm (range: 0.63–1.04 mm) and mean vessel diameter proximal to the implant was 1.75±0.27 mm. Fig. 2 shows an illustrative angiogram from subject 11.

MRI validation of efficacy

All thirteen subjects demonstrated visible hypokinesis in the target myocardial segment on MR cine imaging within two hours of implant deployment. Fig. 3 shows sample MR cine images acquired in subject 2 following implant deployment, analyzed for longitudinal and circumferential strain by semi-automated endocardial border feature tracking. New regions of hypokinesis indicate a reduction in blood supply to the myocardial segment subtended by the implant, as well as the onset of myocardial stunning [26]. Subjects showed significantly decreased circumferential strain in ischemic regions compared to remote regions on Student’s paired t-test (−9.1±5.8% vs −18.3±6.6%, p=0.014).

Subjects that underwent stress perfusion imaging showed a median baseline heart rate of 81 bpm (IQR 80 – 88), SBP of 96 mmHg (IQR 94 – 102), DBP of 55 mmHg (IQR 52 – 59). At peak adenosine stress, subjects showed a median heart rate of 84 bpm (IQR 81 – 89), SBP of 76 mmHg (IQR 74 – 78), DBP of 38 mmHg (IQR 34 – 42) and rate pressure product of 6090 (IQR 5550 – 6500). There were no adenosine stress-induced adverse events. Subjects that underwent adenosine stress first-pass perfusion and LGE MRI each showed perfusion defects in the target myocardial segments without evidence of myocardial infarction. Infarcted myocardium appears hyper-enhanced on LGE images [27]. The absence of myocardial enhancement in target regions with perfusion defects indicates the presence of myocardial ischemia without infarction. Fig. 4a shows an illustrative example from subject 7. A rest perfusion defect is present in the basal to mid anteroseptal wall after deployment of an implant into the proximal LAD. Corresponding LGE images showed no visible myocardial signal enhancement in regions corresponding to the perfusion defect (Fig. 5a). These findings indicate the presence of myocardial ischemia without infarction.

Post-mortem evaluation and gross pathology

Implants were retrieved from the target coronary segment in all subjects except subject 1. This indicates that our method allows investigators to control the implant location within the coronary artery with less concern about distal migration or proximal retraction during balloon removal. Only one of the early subjects showed gross abrasions in the coronary vessel upon visual inspection. Fig. 6 provides an example from subject 9; no gross denudation of the endothelium (Fig. 6b), and no evidence of intraluminal thrombus formation in the implant (Fig. 6c) were observed. Explanted heart tissues from subjects 9 and 13 confirmed the absence of myocardial infarction by TTC staining (Fig. 6d–g).

Discussion

Our proof-of-concept study demonstrates the feasibility and efficacy of a new minimally-invasive and cost-effective percutaneous technique for creating large animal models of acute focal coronary stenosis using 3D printed epicardial coronary implants. Our method enables selective delivery into the arterial segment of interest. The resultant degree of coronary narrowing can be tailored to produce baseline hypoperfusion or vasodilator-induced ischemia without infarction or intraluminal thrombus formation. Our technique has promising applications for validation of new diagnostic MR imaging methods in IHD.

Closed-chest methods for inducing or mimicking atherosclerosis include atherogenic diets [28, 29], partially inflated angioplasty balloons [13, 14], endothelial injury models [10], modified covered stents [11, 12], and intracoronary implanted flow reducers [8]. These methods each have distinct advantages and disadvantages. Atherogenic diets are logistically simple to implement, but can take as long as six months to take effect, and results are unpredictable. Balloon angioplasty techniques are advantageous for modelling acute myocardial ischemia and reperfusion, but pose challenges for models of non-occlusive coronary stenosis. Failure rates due to ventricular fibrillation can be high when complete occlusions are created in ischemia-reperfusion experiments [13]. Endothelial injury models require a waiting period to allow stenosis to develop and do not reliably induce significant

stenoses in all subjects. Covered stents may prove prohibitively expensive, and stents that are not fully expanded pose a risk of collapse, triggering acute thrombosis. Stainless steel stents create MR image artifacts that can completely obscure the vessel of interest and significantly distort the surrounding image [30]. The epicardial coronary flow reducers described by Kraitchman et al. are relatively simple to deploy, but are more challenging to manufacture and are machined individually by hand [8]. They also demonstrate a relatively low success rate of 57% in two studies [8, 9].

Open-chest methods include extracoronary ameroid constrictors, and perfused explanted beating heart models [2, 31]. The most popular method of inducing focal coronary stenosis in swine models remains the ameroid constrictor – a steel or plastic outer sleeve with an inner layer of casein material that swells when positioned around an artery [3, 4, 32]. Ameroid constrictors are difficult to implant: aseptic technique is required, as imaging studies typically follow a recovery period of seven weeks [5]. Placement of ameroid constrictors requires significant surgical expertise and may be operator-dependent with a steep learning curve. Ameroid constrictors reliably induce coronary stenosis, but variability in the rate of casein swelling leads to an inability to precisely control the degree of coronary occlusion [33]. However, the gradual development of the stenosis may be an advantage for chronic studies. The purpose of our technique is not to model the natural history of atherosclerotic disease, but to produce swine models of acute myocardial hypoperfusion for MR imaging studies.

Our new method using 3D printed implants compares favorably with existing methods on logistical simplicity, efficacy, precision and reliability. The outer diameter of the implants was limited to 2.1 mm, but could be varied if needed for larger vessels. The inner diameter was designed to accommodate a deflated, clinically-available coronary angioplasty balloon. We manufactured implants with a range of lengths, allowing investigators to choose a longer implant when more severe stenosis was desired. In the cath lab, we further refined the outer diameter size selection based on the subject's body weight and coronary size estimates at the time of catheterization. Compared to hand-machined nylon flow reducers, these 3D printed implants are simple to manufacture. Stereolithographic 3D printing produces smooth, high quality prints that can be heparin-coated for improved biocompatibility. Our implants are printed on a commercial 3D printer using a standard resin, and can be made in-house or made to order by commercial printing services. 3D printing can be used to produce implants at scale from low-cost materials. This allows investigators to prepare implants with a range of dimensions and select one to fit coronary segment of interest based on intracoronary sizing in the cath lab. If a more precise, subject-specific implant is desired, a coronary CT may be performed and coronary images can be imported into commercially available software for implant design.

Our results are comparable to those reported by Foin et al. using modified covered stents. Our implants induced a mean diameter stenosis of 56.7±7.0%. Foin et al. report a mean diameter stenosis of 54.1±5.9% [11]. Wu et al. report a mean percent diameter stenosis of 91±4% using an endothelial injury model [10]. We achieved a success rate of 75%, which is comparable to other published methods. The method most similar to our technique consists of intracoronary nylon flow reducers, which has a success rate of 57% [8, 9].

Studies using ameroid constrictors typically show a success rate of 80% to 90% [5, 6, 34]. Our overall lower success rate compared to ameroid constrictors may be related to the initial optimization period. Our success rate was 100% after the first five cases. Relative to ameroid constrictors, intracoronary methods may have a higher rate of complications due to the introduction of a foreign body into the coronary vasculature [35]. It is known that swine coronary endothelium is sensitive to vasospasm, and as swine lack collateral vessels, they are more sensitive to sudden severe coronary occlusion [4]. Our study demonstrates that this risk can be managed with an appropriate anticoagulation strategy and use of anti-arrhythmics and nitroglycerin.

Limitations

Our study has several limitations. The measured minimum lumen diameter of the implant-induced coronary narrowing on fluoroscopic images was smaller than the measured inner diameter of the implants following heparin coating. Possible reasons include use of image viewing software rather than quantitative coronary angiography (QCA) software and streaming of contrast or out-of-plane motion. Although the 3D printed implants used in this study can be manufactured in arbitrary dimensions, we ultimately tested a small range of sizes. Likewise, while we used coronary angiography to confirm new coronary stenosis following implant placement, this method can only be used to quantify the geometry of a stenosis. The reference standard for physiologic assessment of stenosis is fractional flow reserve (FFR), measured using coronary pressure wires [36, 37]. Our method can be adapted to include measurement of FFR following implant deployment. Future studies can investigate the correlation of implant size with FFR, which may better characterize the relative severity of stenosis and ischemic burden imposed by implants of varying sizes. While we used multimodal MRI to confirm the location of new perfusion defects in the targeted myocardial segment, we did not distinguish between mild, moderate, and severe perfusion defects or correlate this severity with the implant size or percent diameter stenosis. Future studies may investigate the correlation of post-implant FFR with the extent of myocardial perfusion defects.

Conclusions

Our new method for creating large animal models of focal coronary stenosis opens up new avenues for translational MR imaging studies of myocardial ischemia. This swine model may be used to evaluate novel diagnostic MR imaging methods for IHD or investigations involving the physiological effect of multiple sequential coronary or stenoses in multiple arterial branches. Future work to test a wider range of implant sizes, materials, and resulting physiological measurements are needed. Overall, our rapid prototyping method offers a success rate comparable to that of open-chest delivery of ameroid constrictors, while using percutaneously delivered intracoronary implants.

Acknowledgments:

We thank staff members at the UCLA Lux Lab, the UCLA Translational Research Imaging Center (TRIC) and the Division of Laboratory Animal Medicine at UCLA for their assistance.

Sources of Funding:

This work is supported by American Heart Association Transformational Award 18TPA34170049 and pilot funding from the Department of Radiology and Medicine at UCLA. K.L.N. is supported by funding from the American Heart Association (18TPA34170049), Veterans Health Administration (CX001901), and NIH (HL137562). O.A.A. is supported by NIH (HL142045). P.H. is supported by funding from NIH (HL127153), the American Heart Association (18TPA34170049), and the Veterans Health Administration (CX001901). R.D is supported by funding from NIH (HL133407, HL136578, and HL147133).

Funding:

This work is supported by American Heart Association Transformational Award 18TPA34170049 and pilot funding from the Department of Radiology and Medicine at David Geffen School of Medicine at UCLA.

Data Availability:

The datasets generated during and/or analyzed during the current study are available from the corresponding author on reasonable request.

Nonstandard Abbreviations and Acronyms

FOV	Field of view
IHD	Ischemic heart disease
MRI	Magnetic resonance imaging
TE	Echo time
TI	Inversion time
TR	Repetition time
TTC	Triphenyltetrazolium chloride

REFERENCES

1. Frazier KS, Swindle MM, Clubb FJ, Makin A, & Herron AJ (2011). Swine as Models in Biomedical Research and Toxicology Testing. Veterinary Pathology, 49(2), 344–356. 10.1177/0300985811402846 [PubMed: 21441112]
2. Keeran KJ, Jeffries KR, Zetts AD, Taylor J, Kozlov S, & Hunt TJ (2017). A Chronic Cardiac Ischemia Model in Swine Using an Ameroid Constrictor. Journal of Visualized Experiments, (128). 10.3791/56190
3. Litvak J, Siderides LE, & Vineberg AM (1957). The experimental production of coronary artery insufficiency and occlusion. American Heart Journal, 53(4), 505–518. 10.1016/0002-8703(57)90359-9 [PubMed: 13402712]
4. Hughes GC, Post MJ, Simons M, & Annex BH (2015). Translational Physiology: Porcine models of human coronary artery disease: implications for preclinical trials of therapeutic angiogenesis. Journal of Applied Physiology, 94(5), 1689–1701. 10.1152/japplphysiol.00465.2002
5. Robich MP, Chu LM, Burgess TA, Feng J, Han Y, Nezafat R, … Sellke FW (2012). Resveratrol preserves myocardial function and perfusion in remote nonischemic myocardium in a swine model of metabolic syndrome. Journal of the American College of Surgeons, 215(5), 681–689. 10.1016/j.jamcollsurg.2012.06.417 [PubMed: 22867714]
6. Robich MP, Osipov RM, Nezafat R, Feng J, Clements RT, Bianchi C, … Sellke FW (2010). Resveratrol improves myocardial perfusion in a swine model of hypercholesterolemia

and chronic myocardial ischemia. Circulation, 122(11 SUPPL. 1), S142–S149. 10.1161/CIRCULATIONAHA.109.920132 [PubMed: 20837905]

7. Sabe AA, Elmadhun NY, Robich MP, Dalal RS, & Sellke FW (2013). Does resveratrol improve insulin signaling in chronically ischemic myocardium? Journal of Surgical Research, 183(2), 531–536. 10.1016/j.jss.2013.03.004 [PubMed: 23622724]
8. Kraitchman D, Bluemke D, Chin B, & Heldman A. (2000). A minimally invasive method for creating coronary stenosis in a swine model for MRI and SPECT imaging. Investigative Radiology, 35(7), 445–451. 10.1097/00004424-200007000-00008 [PubMed: 10901107]
9. Gerber BL, Boston RC, Kraitchman DL, Chin BB, Lima JAC, Bluemke DA, & Heldman AW (2007). Single-Vessel Coronary Artery Stenosis: Myocardial Perfusion Imaging with Gadomer-17 First-Pass MR Imaging in a Swine Model of Comparison with Gadopentetate Dimeglumine. Radiology, 225(1), 104–112. 10.1148/radiol.2251011377
10. Wu M, Bogaert J, D'Hooge J, Sipido K, Maes F, Dymarkowski S, … Claus P. (2010). Closed-chest animal model of chronic coronary artery stenosis. Assessment with magnetic resonance imaging. International Journal of Cardiovascular Imaging, 26(3), 299–308. 10.1007/s10554-009-9551-1 [PubMed: 20012206]
11. Foin N, Sen S, Petraco R, Nijjer S, Torii R, Kousera C, … Davies J. (2013). Method for Percutaneously Introducing, and Removing, Anatomical Stenosis of Predetermined Severity In Vivo: The "Stenotic Stent." Journal of Cardiovascular Translational Research, 6(4), 640–648. 10.1007/s12265-013-9476-x [PubMed: 23733543]
12. Rissanen TT, Nurro J, Halonen PJ, Tarkia M, Saraste A, Rannankari M, … Ylä-Herttuala S. (2013). The bottleneck stent model for chronic myocardial ischemia and heart failure in pigs. American Journal of Physiology - Heart and Circulatory Physiology, 305(9), 1297–1308. 10.1152/ajpheart.00561.2013
13. Krombach GA, Kinzel S, Mahnken AH, Günther RW, & Buecker A. (2005). Minimally invasive close-chest method for creating reperfused or occlusive myocardial infarction in swine. Investigative Radiology, 40(1), 14–18. [PubMed: 15597015]
14. Nguyen K-L, Shao J, Ghodrati VK, Ajijola OA, Dharmakumar R, Finn JP, & Hu P. (2019). Ferumoxytol-Enhanced CMR for Vasodilator Stress Testing: A Feasibility Study. JACC: Cardiovascular Imaging, 12(8), 1582–1584. 10.1016/j.jcmg.2019.01.024 [PubMed: 30878418]
15. Giannopoulos AA, Mitsouras D, Yoo SJ, Liu PP, Chatzizisis YS, & Rybicki FJ (2016). Applications of 3D printing in cardiovascular diseases. Nature Reviews Cardiology, 13(12), 701–718. 10.1038/nrcardio.2016.170 [PubMed: 27786234]
16. Oliveira-Santos M. de, Oliveira-Santos E, Gonçalves L, & Silva Marques J. (2019). Cardiovascular Three-Dimensional Printing in Non-Congenital Percutaneous Interventions. Heart Lung and Circulation, 28(10), 1525–1534. 10.1016/j.hlc.2019.04.020
17. Forte MNV, Hussain T, Roest A, Gomez G, Jongbloed M, Simpson J, … Valverde I. (2019). Living the heart in three dimensions: Applications of 3D printing in CHD. Cardiology in the Young, 29(6), 733–743. 10.1017/S1047951119000398 [PubMed: 31198120]
18. Alonzo M, AnilKumar S, Roman B, Tasnim N, & Joddar B. (2019). 3D Bioprinting of cardiac tissue and cardiac stem cell therapy. Translational Research, 211, 64–83. 10.1016/j.trsl.2019.04.004 [PubMed: 31078513]
19. Lee W, Hong Y, & Dai G. (2019). 3D bioprinting of vascular conduits for pediatric congenital heart repairs. Translational Research, 211, 35–45. 10.1016/j.trsl.2019.03.007 [PubMed: 31034816]
20. Hollowed JJ, Colbert CM, Currier JW, & Nguyen K-L (2020). Novel Percutaneous Approach for Deployment of 3D Printed Coronary Stenosis Implants in Swine Models of Ischemic Heart Disease. Journal of Visualized Experiments, e60729. 10.3791/60729
21. Shaw LJ, Berman DS, Maron DJ, Mancini GBJ, Hayes SW, Hartigan PM, … Boden WE (2008). Optimal medical therapy with or without percutaneous coronary intervention to reduce ischemic burden: results from the Clinical Outcomes Utilizing Revascularization and Aggressive Drug Evaluation (COURAGE) trial nuclear substudy. Circulation, 117(10), 1283–1291. 10.1161/CIRCULATIONAHA.107.743963 [PubMed: 18268144]
22. Liu A, Wijesurendra RS, Liu JM, Greiser A, Jerosch-Herold M, Forfar JC, … Ferreira VM (2018). Gadolinium-Free Cardiac MR Stress T1-Mapping to Distinguish Epicardial From Microvascular

Coronary Disease. Journal of the American College of Cardiology, 71(9), 957–968. 10.1016/j.jacc.2017.11.071 [PubMed: 29495995]

23. Husso M, Nissi MJ, Kuivanen A, Halonen P, Tarkia M, Teuho J, … Toÿräs J. (2019). Quantification of porcine myocardial perfusion with modified dual bolus MRI-A prospective study with a PET reference. BMC Medical Imaging, 19(1), 1–11. 10.1186/s12880-019-0359-8 [PubMed: 30611240]
24. Fishbein MC, Meerbaum S, Rit J, Lando U, Kanmatsuse K, Mercier JC, … Ganz W. (1981). Early phase acute myocardial infarct size quantification: Validation of the triphenyl tetrazolium chloride tissue enzyme staining technique. American Heart Journal, 101(5), 593–600. 10.1016/0002-8703(81)90226-X [PubMed: 6164281]
25. Fieno DS, Kim RJ, Chen EL, Lomasney JW, Klocke FJ, & Judd RM (2000). Contrast-enhanced magnetic resonance imaging of myocardium at risk: Distinction between reversible and irreversible injury throughout infarct healing. Journal of the American College of Cardiology, 36(6), 1985–1991. 10.1016/S0735-1097(00)00958-X [PubMed: 11092675]
26. Lindsey ML, Bolli R, Canty JM, Du X-J, Frangogiannis NG, Frantz S, … Heusch G. (2018). Guidelines for experimental models of myocardial ischemia and infarction. American journal of physiology. Heart and circulatory physiology, 314(4), H812–H838. 10.1152/ajpheart.00335.2017 [PubMed: 29351451]
27. Mahrholdt H, Wagner A, Judd RM, Sechtem U, & Kim RJ (2005, August). Delayed enhancement cardiovascular magnetic resonance assessment of non-ischaemic cardiomyopathies. European Heart Journal. Eur Heart J. 10.1093/eurheartj/ehi258
28. Liao J, Huang W, & Liu G. (2016). Animal models of coronary heart disease. Journal of Biomedical Research, 30(1), 3–10. 10.7555/jbr.30.20150051
29. Tanimoto A, Kawaguchi H, Yoshida H, Misumi K, Fujiki M, Miyoshi N, … Miura N. (2011). Microminipig, a Non-rodent Experimental Animal Optimized for Life Science Research: Novel Atherosclerosis Model Induced by High Fat and Cholesterol Diet. Journal of Pharmacological Sciences, 115(2), 115–121. 10.1254/jphs.10r17fm
30. Adams GJ, Baltazar U, Karmonik C, Bordelon C, Lin PH, Bush RL, … Morrisett JD (2005). Comparison of 15 different stents in superficial femoral arteries by high resolution MRI ex vivo and in vivo. Journal of Magnetic Resonance Imaging, 22(1), 125–135. 10.1002/jmri.20359 [PubMed: 15971171]
31. Schuster A, Sinclair M, Zarinabad N, Ishida M, Van Den Wijngaard JPHM, Paul M, … Chiribiri A. (2015). A quantitative high resolution voxel-wise assessment of myocardial blood flow from contrast-enhanced first-pass magnetic resonance perfusion imaging: microsphere validation in a magnetic resonance compatible free beating explanted pig heart model. European Heart Journal Cardiovascular Imaging, 16(10), 1082–1092. 10.1093/ehjci/jev023 [PubMed: 25812572]
32. Elzinga WE (1969). Ameroid constrictor: uniform closure rates and a calibration procedure. Journal of Applied Physiology, 27(3), 419–421. 10.1152/jappl.1969.27.3.419 [PubMed: 5804143]
33. Inou T, Tomoike T, Watanabe K, Kikuchi Y, Mizukami M, Kurozumi T, & Nakamura M. (1980). A newly developed X-ray transparent ameroid constrictor for study on progression of gradual coronary stenosis. Basic Research in Cardiology, 75(4), 537–543. 10.1007/BF01907835 [PubMed: 7436997]
34. Guo M, Liu J, Guo F, Shi J, Wang C, Bible PW, … Shi D. (2018). Panax Quinquefolium Saponins Attenuate Myocardial Dysfunction Induced by Chronic Ischemia. Cellular Physiology and Biochemistry, 49(4), 1277–1288. 10.1159/000493407 [PubMed: 30205393]
35. Biran R, & Pond D. (2017). Heparin coatings for improving blood compatibility of medical devices. Advanced Drug Delivery Reviews, 112, 12–23. 10.1016/j.addr.2016.12.002 [PubMed: 28042080]
36. Bressi E, Mangiacapra F, Morisco C, Barbato E, & Sticchi A. (2018). Fractional flow reserve (FFR) as a guide to treat coronary artery disease. Expert Review of Cardiovascular Therapy, 16(7), 465–477. 10.1080/14779072.2018.1489236 [PubMed: 29923434]

Clinical Relevance:

Reliability of closed-chest techniques to create swine models of acute coronary stenosis remains limited. This work demonstrates the feasibility and efficacy of a rapid prototyping method using 3D printed, heparin-coated, coronary stenosis implants to percutaneously create swine models of myocardial hypoperfusion and ischemia, which can be used to evaluate novel diagnostic MRI methods for ischemic coronary heart disease.

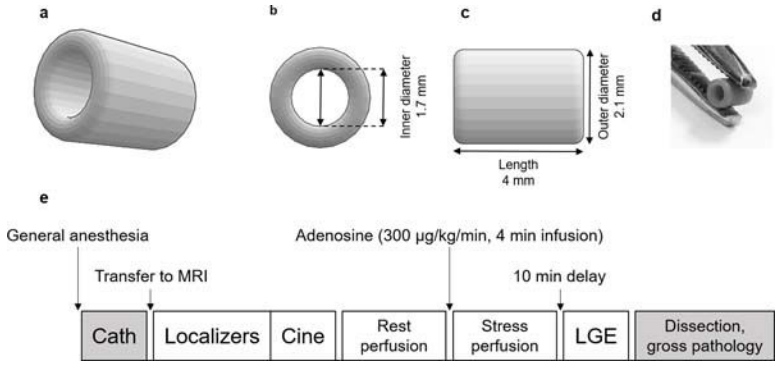

Fig. 1. Design of 3D-printed coronary implant and MR imaging protocol.

Oblique view **(a)**, short-axis cross-sectional view **(b)** and long-axis side view **(c)** of an implant design (2.1 mm outer diameter, 1.7 mm inner diameter and 4.0 mm length) are shown. The printed 3D implant is shown in **(d)**. Following catheterization, subjects were transferred to MRI suite for imaging **(e)**

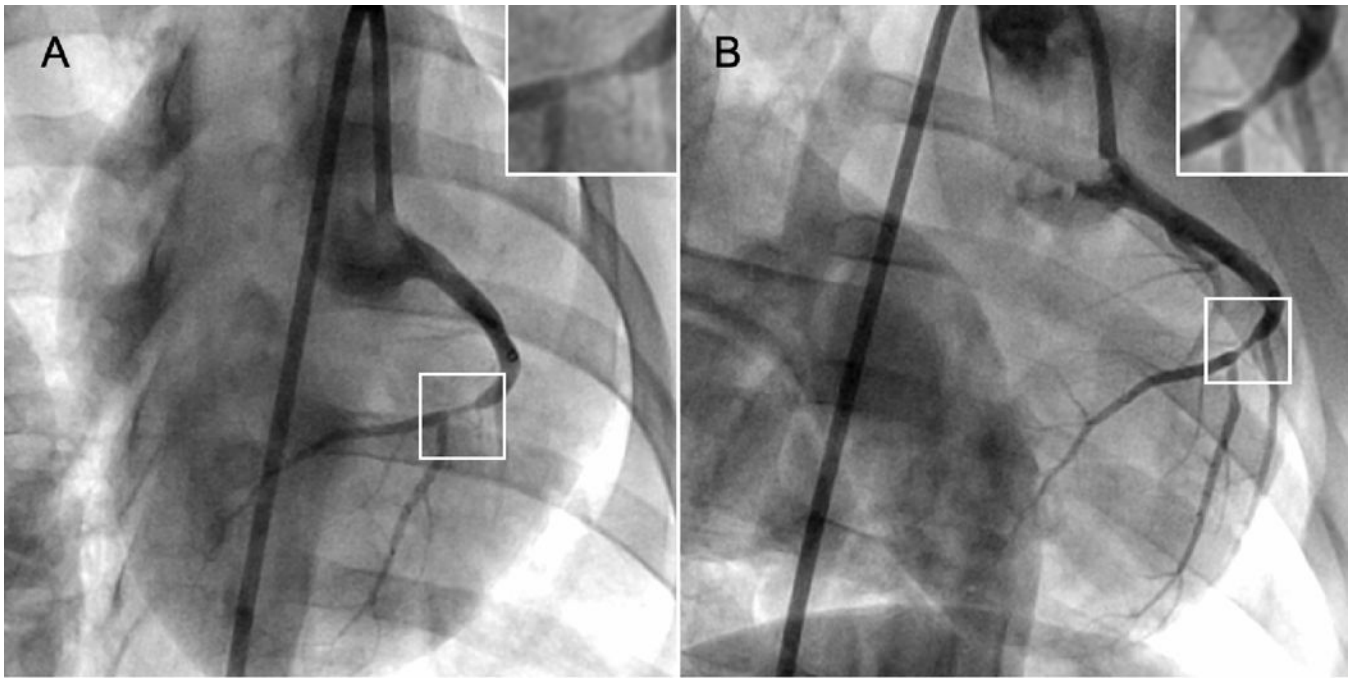

Fig. 2. Orthogonal fluoroscopic images.

Posteroanterior (PA, **a**) and left anterior oblique (LAO 40°, **b**) views from subject 11 show visible arterial narrowing (inserts) following deployment of the implant into the left anterior descending artery. Minimum lumen diameter 0.85 mm, percent diameter stenosis 59%

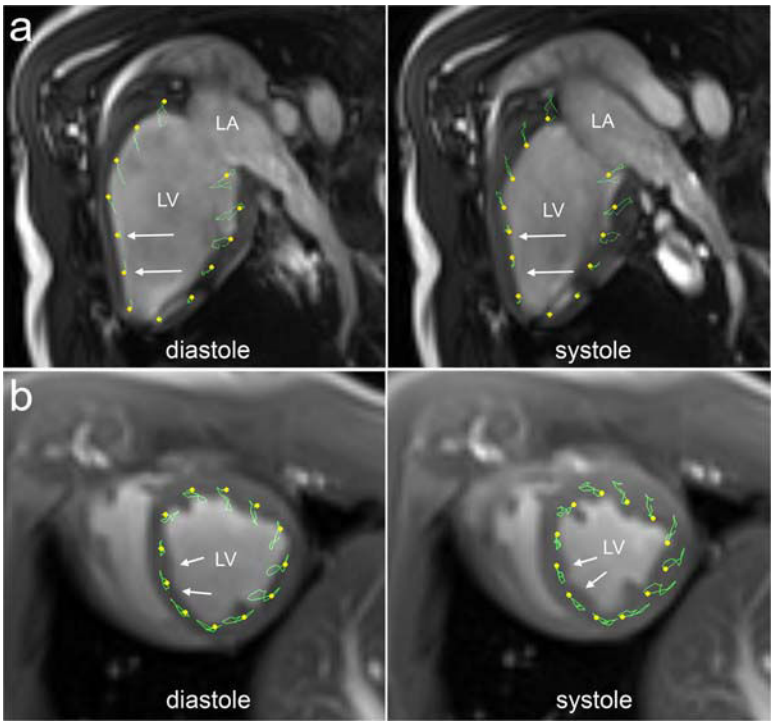

Fig. 3. Illustrative cine MR images of a swine with a 3D-printed coronary stenosis implant in the left anterior descending artery.

Two-chamber **(a)** and short-axis **(b)** left ventricular cine MR images from subject 2 show mid to distal left ventricular anterior and septal hypokinesis (white arrows). Compared to remote (unaffected) segments, there was reduction of longitudinal strain (−17.0% vs −3.9%) and circumferential strain (−23.8% vs −6.5%) in the hypoperfused /ischemic (affected) segments using endocardial border feature-tracking (TomTec, 2D CPA MR). Left ventricle (LV), left atrium (LA)

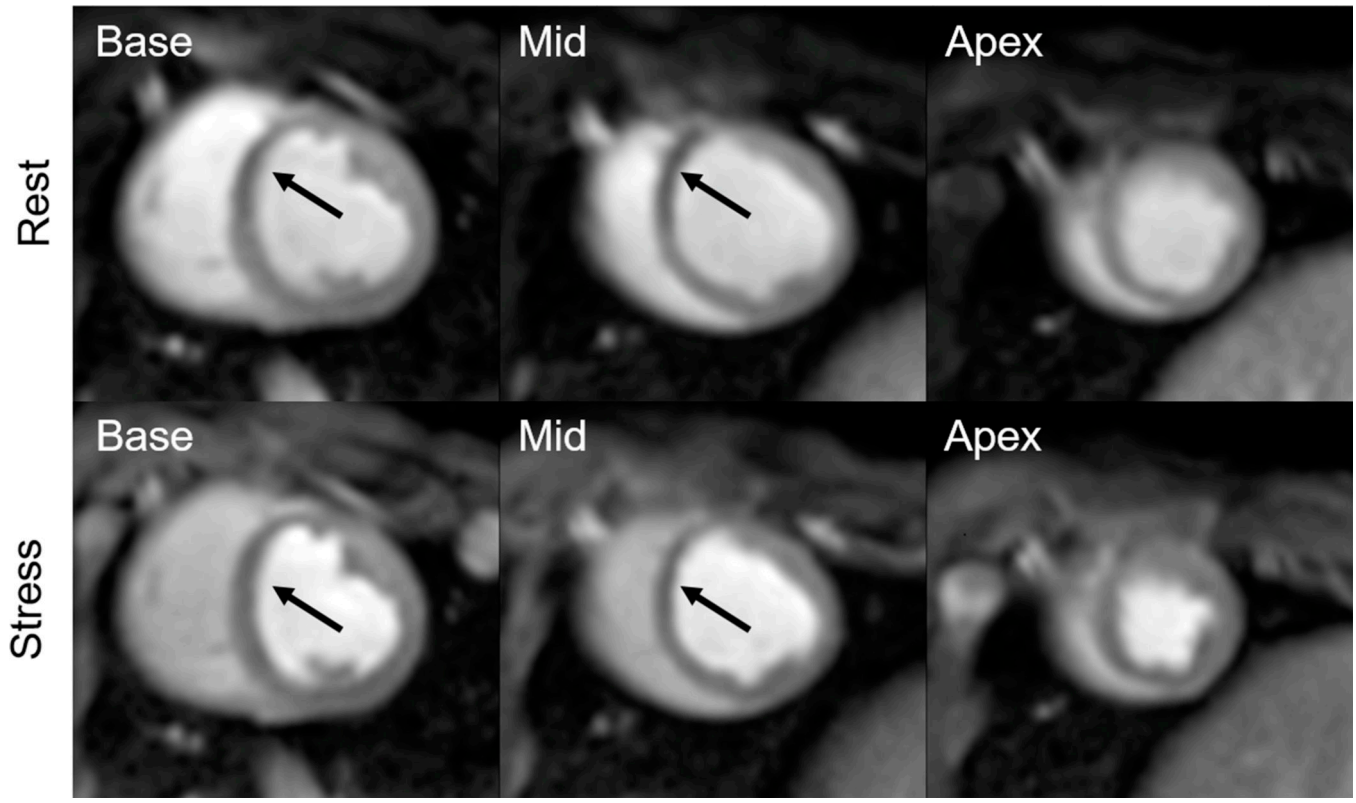

Fig. 4. Gadolinium-enhanced rest and stress first pass perfusion images.

Perfusion defect (arrows) is present in the basal to mid anteroseptal to inferior wall in subject 7 (LAD, **a**). Perfusion defect (arrows) is present in the basal to mid inferolateral wall in subject 9 (LCX, **b**)

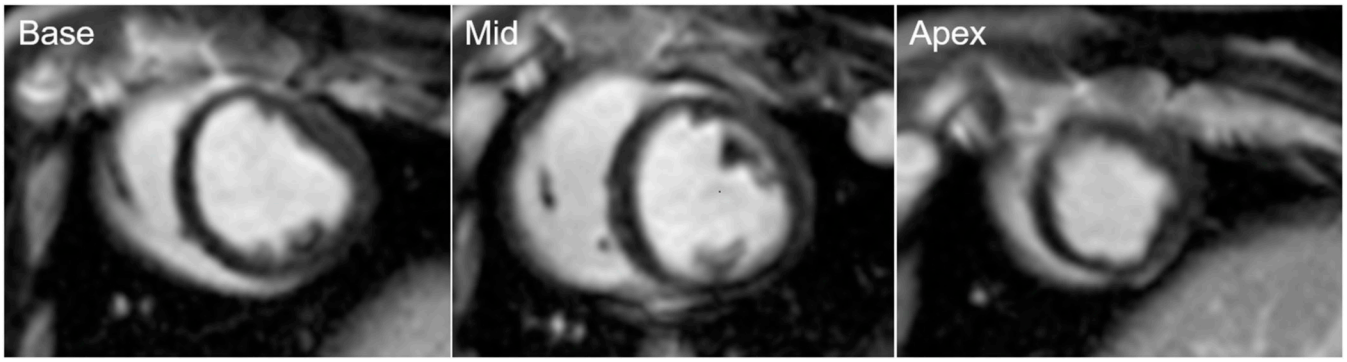

Fig. 5. Late gadolinium-enhanced images (base, mid, apex) using a phase-sensitive inversion recovery gradient echo sequence.

No evidence of myocardial infarction is visible in myocardial segments subtended by the left anterior descending coronary artery (subject 7, **(a)**) or the left circumflex artery (subject 9 **(b)**)

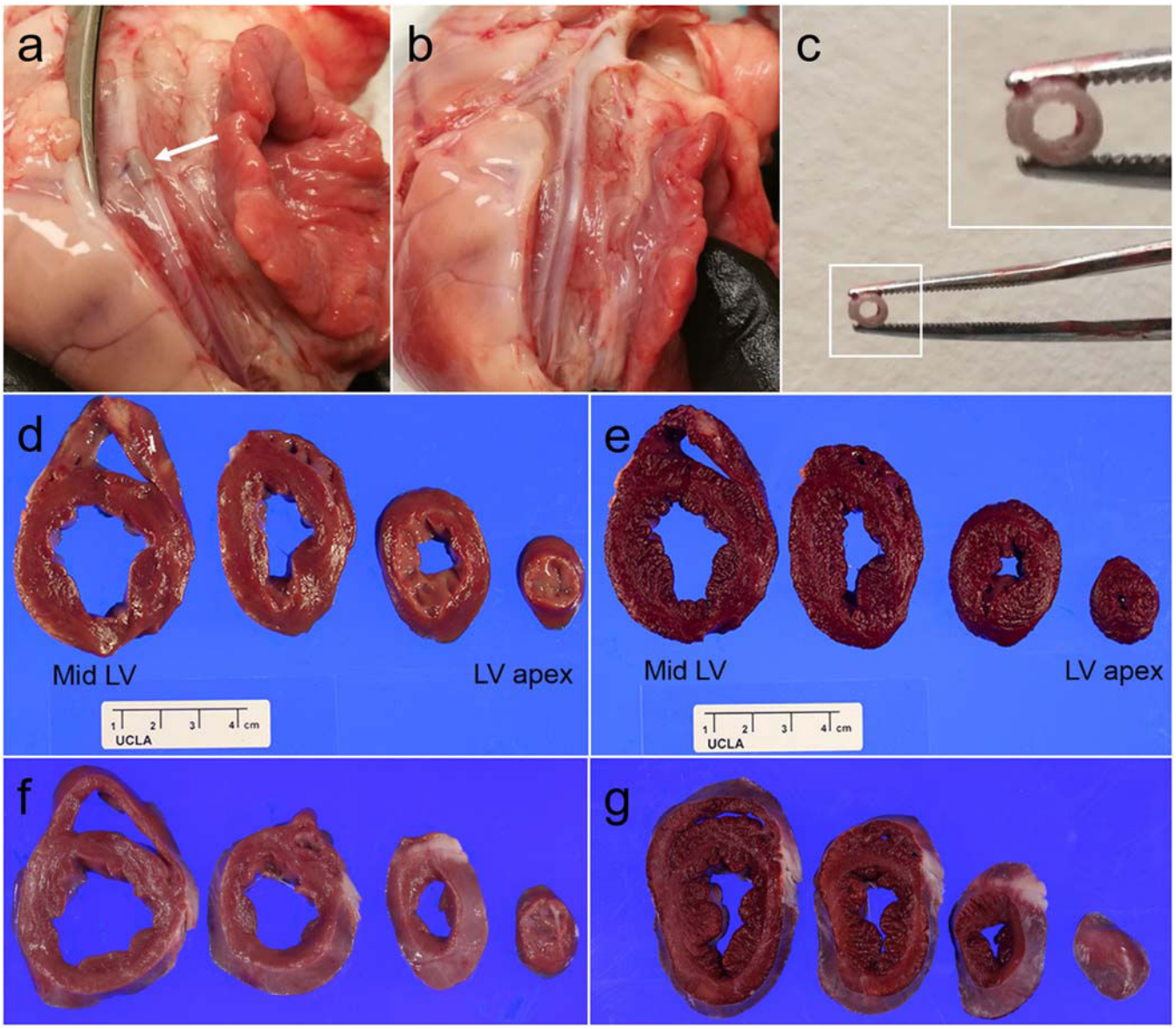

Fig. 6. Retrieval of epicardial coronary implants from subjects 9 and 13.

The implant in subject 9 is seen in the left circumflex artery (white arrow, **a**). There is no evidence of gross denudation of the endothelium (**b**). Inspection of the implant showed lack of thrombus formation (**c**, cross-sectional view with magnified insert). Gross specimen (**d**) and triphenyltetrazolium chloride staining (**e**) from subject 9 showed no evidence of myocardial tissue infarction in the left ventricle (LV). Gross (**f**) and stained (**g**) specimen from subject 13 likewise showed no evidence of infarction.

Table 1.

Summary of implant deployment procedures and results

Subject	Location of implant	Size of implant* (OD, ID, L [mm])	Implant retrieved	Animal survived	Implant retrieved and animal survived
1	LAD	2.1, 1.5, 4	--	✓	--
2	LAD	1.5, 1.1, 4	✓	✓	✓
3	LCX	2.1, 1.5, 2.6	✓	--	--
4	LAD	2.1, 1.5, 4	✓	✓	✓
5	LAD	2.1, 1.5, 4	✓	--	--
6	LAD	2.1, 1.5, 4	✓	✓	✓
7	LAD	2.1, 1.5, 4	✓	✓	✓
8	LAD	2.1, 1.5, 4	✓	✓	✓
9	LCX	2.1, 1.5, 4	✓	✓	✓
10	LAD	2.1, 1.5, 4	✓	✓	✓
11	LAD	2.1, 1.5, 4	✓	✓	✓
12	LAD	2.1, 1.5, 4	✓	✓	✓
13	LAD	2.1, 1.5, 4	✓	✓	✓

*Mean deviation from nominal implant dimensions of −0.03±0.07 mm in length, 0.00±0.06 mm in outer diameter and −0.39±0.06 mm in inner diameter following application of the heparin coating. On average, heparin coating caused a decrease in implant inner diameter of 0.09±0.11 mm.

ID, inner diameter; LAD, left anterior descending artery; LCX, left circumflex artery; L, length; mm, millimeter; OD, outer diameter